Controlled Demolition of High-Rise RC Industrial Chimney

In-Use Overturning Method

João Mário Rodrigues Bento

mariobento957@gmail.com

Department of Civil Engineering, Architecture and Georesources, Instituto Superior Técnico, University of Lisbon

Av. Rovisco Pais, 1049-001 Lisboa, Portugal

September 2021

Abstract

There are technical difficulties in the conventional mechanical demolition process of tall chimneys. Not to mention the added restraints of occasional space limitations around the chimney and the long time, safety requirements and the high-costs that process can involve. The recommended efficient method to demolish tall chimneys is the controlled demolition using explosives.

To generalize, demolition blasting refers to the controlled blasting technology used for removing tall and abandoned structures. The basic principles of demolition blasting are to eliminate critical elements of the structure by blasting and consequent collapse. To facilitate this process, a structural pre-weakening work shall be done prior to blasting.

Accordingly to this concept, an implosion method is proposed considering a wedge-shaped notch that shall be blasted out to create a plastic hinge. Then, the structure will turn to a kinematic mechanism and will collapse.

Keywords: controlled demolition, blasting, implosion, industrial chimney

1 Introduction

1.1 Background

The thermo-electrical plant located at Mitrena, in the right bank of River Sado, five kilometres distant from City of Setúbal (Portugal), ended operations after a life-time of thirty-five years due to environmental reasons. In 2020, the controlled demolition of the high-rise reinforced concrete chimneys was carried out.

Figure 1.1: Thermo-electrical plant view (Google Earth)

The conventional method of demolition leads to the well-known mechanical demolition needing the support of heavy equipment and long-time duration of on-site activities. For tall structures, it is a non-competitive (time and costs) solution. Therefore, blasting demolition is the acceptable cost-efficient method.

An additional advantage of controlled collapse is to minimize the risk of demolished fragments impact and cause damage to the neighboring structures. The method allows to confine debris in the plant and facilitate further dismantling and transportation to recycling site.

However, hazards may be present and shall be attended during the design phase to avoid any unwanted incidents such as failure in the wrong direction, squatting or incomplete failure and the possibility of parts of the structure be separated in the fall.

1.2 Objectives

The case study is analyzed and discussed on the basis of theory of structures but limited to the chimney stack structure designated as C1. Analysis of structural safety and calculations for ultimate limit states approach are achieved in two differentiate design situations:

- Ex-ante phase: before blasting occurs and linked to the time lag necessary to spend in structural pre-weakening.
- Ex-post phase: sequent to implosion followed by the plastic hinge formation, cinematic mechanism and collapse.

To note it is not included in present dissertation:

- The analysis of structure mechanics in the cinematics of tipping movement lap.
- The blast design and analysis of the structure under blast load simulation.

1.3 Case study – RC *Chimney C1*

The stack has a 201 m total height with variable cross-section. Outer diameter is 14.810 m, at ground level, and 7.172 m, at the free extremity. The width of shell varies in the range of 700 mm (bottom) to 200 mm (top). Prescribed concrete strength is Grade C30/37.

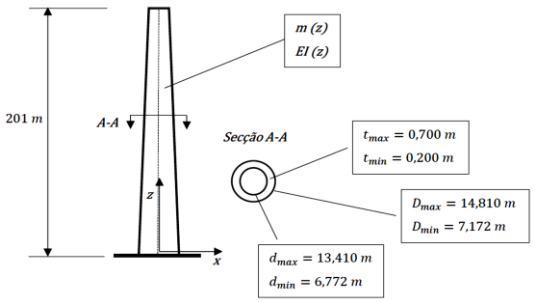

Figure 1.2: Geometrical properties of the stack

Reinforcement bars Grade S400 are arranged into two circumference layers with pre-defined 25 mm nominal diameter for longitudinal bars.

2 Actions and effects

2.1 Actions modelling

The ultimate limit states design requires first the modelling of actions or the load models for each specific design situation.

- Gravity Loads (*G*): structural and non-structural self-weight.
- Variable action (*Q*): climate wind action.
- Earthquake (A_E): seismic action.
- Accidental (*A*): implosion action.

To resume, appropriate arrangement of actions shall be associated with material properties and geometrical data for ULS design purpose in line with a specific design situation.

2.2 Gravity loads effect

Structural concrete of $25\ kN/m^3$ (including shell and support inner rings at intermediate levels); and thermal insulation coating of $22\ kN/m^3$.

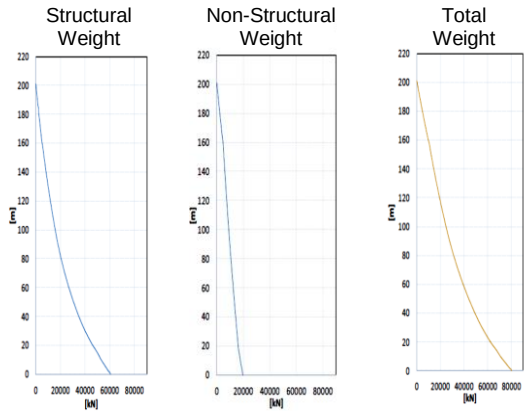

Figure 2.1: Axial forces by gravity load effect

$$N_s = 80180\ kN$$

MS EXCEL is used for numeric calculations and plotting diagrams.

2.3 Climate wind effect

Wind dynamic peak pressure results from the amplification of average dynamic wind pressure by effect of short-term wind velocity fluctuations.

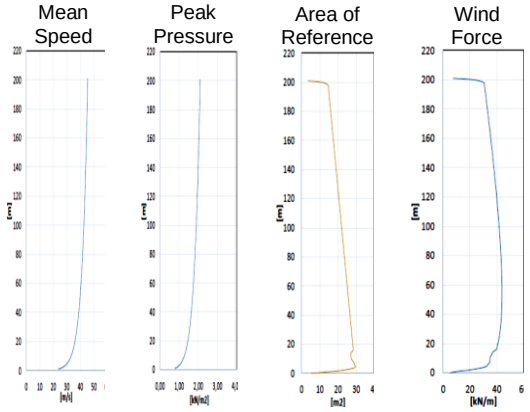

Figure 2.2: Velocity, peak pressure and force profiles

The determination of $c_s c_d$ require of numerical solution of aerodynamic parameters, as follows:

- Force factor (global effect).
- Damping logarithmic decrement.
- Quasi-static response factor.
- Resonance response factor.

The structural behavior factor is $c_s c_d = 0.905$. Wind load case (global effect) is as follows:

$$F_{WS} = c_s c_d \cdot c_f \cdot q_p(z_e) \cdot A_{ref}$$

This method considers effects of dynamic wind load using a quasi-static analysis, based on the fundamental frequency of the structure and its damping factor.

Aerodynamic parameters refer to the turbulence and amplification of peak pressure by means of the response gust factor.

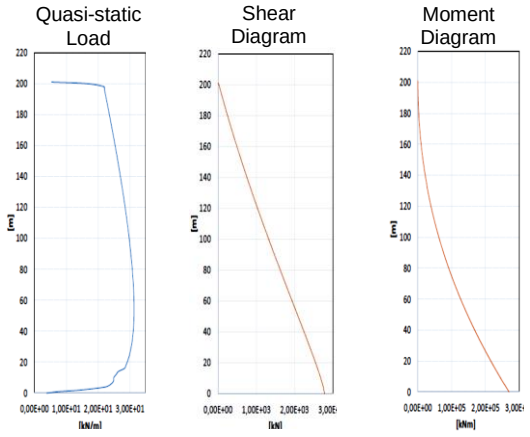

Figure 2.3: Moments and shear forces by wind load effect

Maximum effects at $z = 0.0\ m$ cross-section:

$$M_s = 270000\ kNm;\ V_s = 2784\ kN$$

2.4 Dynamic interferences

In the case of two cylinders distant each other and subjected to wind load action, if the cylinder at downwind is outside the influence of track turbulence zone, aerodynamic interference is nil and each cylinder has aerodynamic behaviour free of interference. This effect exists when the two cylinders are sufficiently close or downwind cylinder stays in the track turbulence zone.

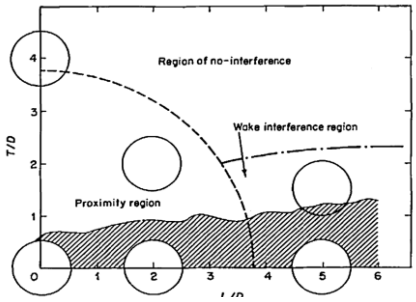

Figure 2.4: Aerodynamic interference classification [17]

The arrangement of the two chimneys defines a 50º angle alignment relative to O-E direction. Using EC-1-4 approach results $k = 1.095$ then, along wind critical attack angle, the force factor shall be amplified ($c_f = c_{f,0} \cdot \psi_\lambda \cdot k = 0.863$). Herein in-use method of analysis considers a mono-modal excitation model, and most severe load case associates the turbulence originated by wind along longitudinal direction.

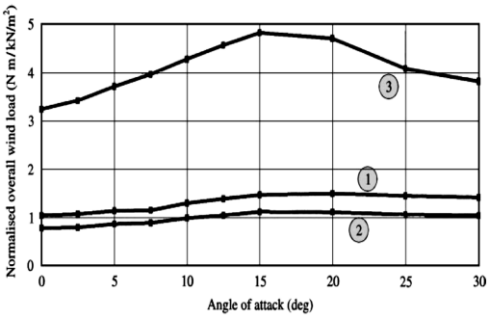

Figure 2.5: Interference and critical wind direction [14]

It is assumed that a lag of wind directions can originate the maximum answer of the structure resulting the higher value (or values close to the higher value) of wind forces effect:

$$\theta_{crit} = [0° \div 30°]$$

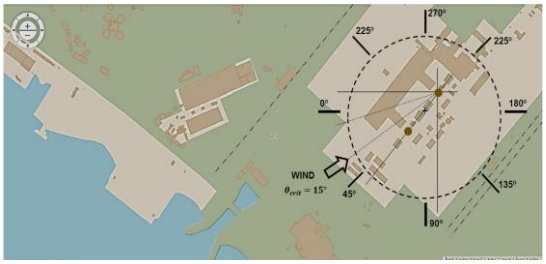

Figure 2.6: Critical wind direction (WebSIG)

Critical wind direction to be OSO - SO sector.

2.5 Vortex shedding effect

The structure may experiment excitation mode and significant bending effect, transverse to the wind direction. The effects of this vibration may be evaluated considering that inertia forces and elastic deformation forces in equilibrium.

$$F_{w,t}(z) = m(z) \cdot (2 \cdot \pi \cdot n_{i,y})^2 \cdot \Phi_{i,y}(z) \cdot y_{F,max}$$

The maximum transverse displacement $y_{F,max}$ is a parameter associated to top level diameter:

$$y_{F,max}/b = 0.093 < 0{,}1 \rightarrow y_{F,max} = 0.67\ m$$

Numeric calculations are according to Eurocode 1-4, Method 1, based on Ruscheweyh Model.

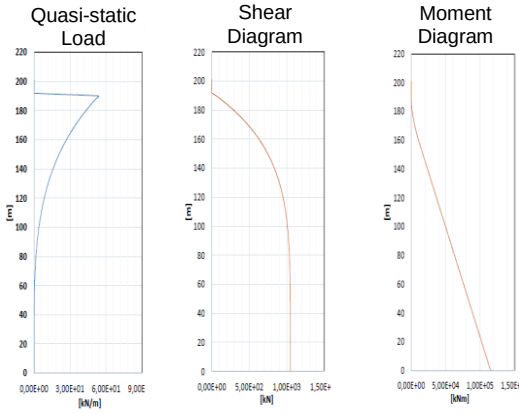

Figure 2.7: Moments and shear forces by vortex effect

Maximum effects at $z = 0.0\ m$ cross-section:

$$M_s = 105100\ kNm;\ V_s = 994\ kN$$

2.6 Wind added effects

The added effects of wind shall be considered as inputs for ULS using SRSS rule to determine the resultant of wind effect components.

$$S = \sqrt{S_1^2 + S_2^2}$$

2.7 Seismic effect

Seismic intensity classification is represented by the reference maximum ground acceleration a_{gr} according to geographical location (zone 3) and type of seismic action. For different values of return period (475 y.) and probability factor (0.10 over 50 y.), the ground acceleration shall be related to maximum reference acceleration. A return-period of (95 y.) is herein considered.

$$a_{gc} = a_{gr} \left[\frac{T_{RC}}{T_{NCR}} \right]^k$$

$a_{g,95} = 0.5 \frac{m}{s^2}$; seism type 1

$a_{g,95} = 0.9 \frac{m}{s^2}$; seism type 2

Structural ductility factor $q = 1.5$ (DCL).

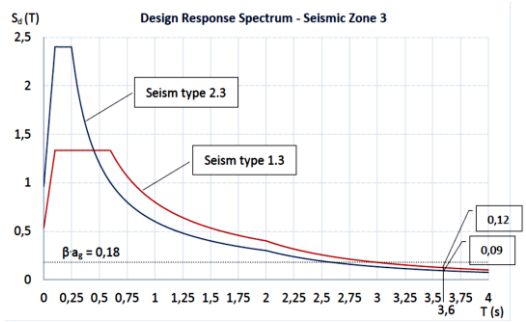

Figure 2.8: Elastic design response spectrum

Considering that the response of the structure for each vibration mode can be modelled by a SDOF system, the upper limit of total response can be obtained by modal combination.

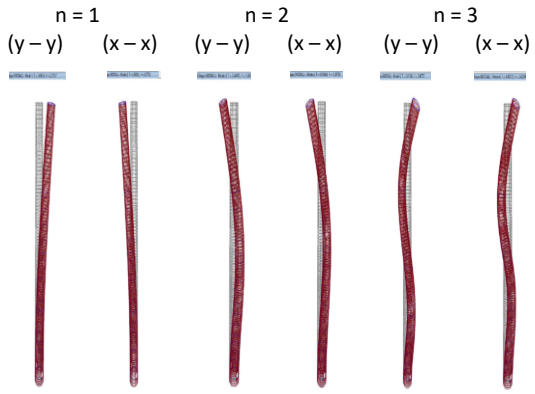

Figure 2.9: First three free vibration modes (SAP2000)

First-mode natural vibration period is $T = 3.69s$ (y-y direction) and $T = 3.60s$ (x-x direction).

Maximum effects at $z = 0.0\ m$ cross-section:

$$M_s = 111734\ kNm;\ V_s = 2065\ kN$$

2.8 Design scenarios

Transient design situation: refers to structural pre-weakening period (~ 6 months). It considers STR ultimate limit state:

$$E_d \leq R_d$$

No failure shall occur during transient situation.

Seismic design situation: refers to the period of transient situation. Accordingly, it considers the strength ultimate state (STR) to seismic action.

Accidental design situation: refers to immediate period after the implosion and hinge formation. It considers the strength ultimate state (STR) to make sure that failure of concrete occurs:

$$E_d > R_d$$

And the equilibrium ultimate state (EQU), i.e. the stack overturning around the plastic hinge:

$$E_{d,dst} > E_{d,stb}$$

3 Pre-weakening criteria

3.1 Geometric parameters

Structural pre-weakening includes the opening of two triangle-shaped opposite windows and a borehole mesh in the implosion notch for the insertion of explosive load. On the opposite side of the notch, outer reinforcement layer is cut-off.

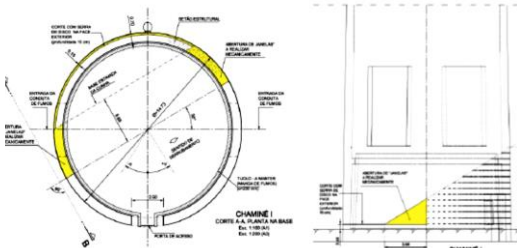

Figure 3.1: Structural pre-weakening definition [15]

Geometrical modelling of implosion notch shall attend to two parameters:

- The angle θ defined in horizontal plane by the residual section after implosion.
- The angle δ the inclined shell curvature of the upper edge of implosion notch.

The variations of one or both parameters, in-between appropriate limits, influence structural behavior after implosion.

On the opposite side of the notch, an horizontal cut of 150 mm depth in the shell, all along pre-defined angle θ = 120º, reduces concrete area and disrupts longitudinal reinforcement in the outer layer of this transverse section segment.

3.2 Properties modification

Before implosion, in-plane failure pre-weakened section maintains a uniform compression state by the effect of permanent gravity loads. This condition will change sharply immediately after implosion.

The original cross-section is decreased by a large amount and the residual section serves for some moments as a support to the stack.

The center of gravity of residual cross-section segment moves away from the stack center-line creating significant eccentricity for the resultant of permanent load.

During this very short time ($t_1 < 1\ s$), stress distribution self-modifies and advances rapidly to plastic state.

4 Design in transient situation

There is uncertainty about the diameter size of bars of longitudinal reinforcement. Additionally, the concrete strength in the implosion notch is decreased due to insert borehole mesh. So it is justified to examine different strength scenarios.

Table 4.1: Scenarios for (STR) design analysis

Grade S400	Grade C30/37	Grade C35/45
Φ25 mm	D	A
Φ20 mm	C	B

Scenario C fits to minimum strength condition as it considers a 20 mm diameter size (in accord with in situ test specimen) instead of 25 mm (as per construction drawings) and is conservative about the concrete strength of implosion notch. The failure surface of residual section by using program GalaReinforcement (Alashki, I., 2002).

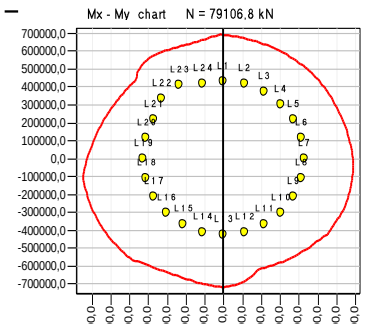

Figure 4.1: Failure surface (Scenario C)

Axial force design value: $N_{sd} = 79107\ kN$

Failure surface critical interaction point:

$$(M_{x,Rd}; M_{y,Rd}) = (-471051; 429299)\ kNm$$

Therefore, the ultimate strength factor:

$$\frac{M_{ult}}{M_{res}} = 1.360$$

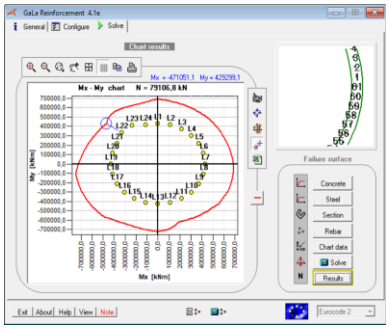

Figure 4.2: Strength critical interaction (Scenario C)

Then structural safety is verified for scenario C. The strength downgrade from Grade C35/45 to C30/37 slightly reduces the ultimate strength factor (for the equal value of axial load).

5 Post-implosion analysis

5.1 Strength ultimate limit state

During the effect of implosion, the stack shall not experiment instantaneous failure or suffer squatting or any other local instability, hence failure process must occur gradually.

However the effect of these impulsive forces are transient and short-time duration with high values of strain rate.

This condition generates dynamic increase on compression concrete properties which value must be evaluated.

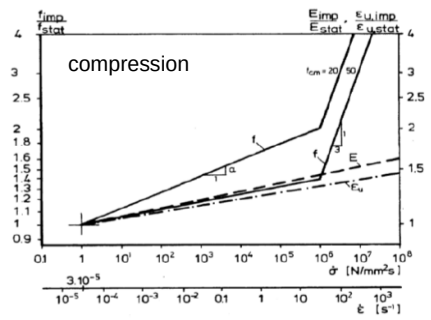

Figure 5.1: Influence of strain rate on compression [3]

It is considered to be $DIF = [1.6 \div 1.8]$ as a first-cut evaluation of this effect.

In addition to this, measures taken from a real-case of chimney controlled demolition made evidence of a dynamic load factor that shall be considered to fit to real deformation results as derived from the statics analysis [2].

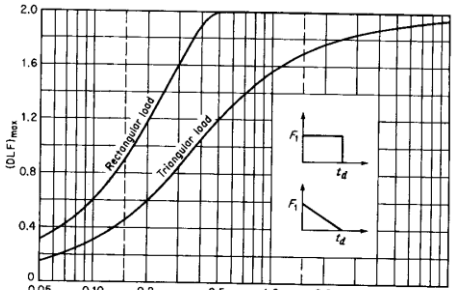

Figure 5.2: Maximum structure elastic response [1]

It is considered to be $DLF = [1.15 \div 1.20]$ as a representative gap of this amplification.

Table 5.1: Data for (STR) design analysis

Grade	DIF	DLF	Load Case 1	Load Case 2
C80/95	1,8	1,15	*100070 **590514	81875 483148
C45/55 C50/60	---	---	87018 513490	71196 420128

*Axial Force (kN); ** Bending Moment (kNm)

Dynamic structural answer:

In the brief moment following the implosion prevails the dynamic effect of the detonation wave propagation in structure response, the limit state condition must verify: $R_d > E_d$.

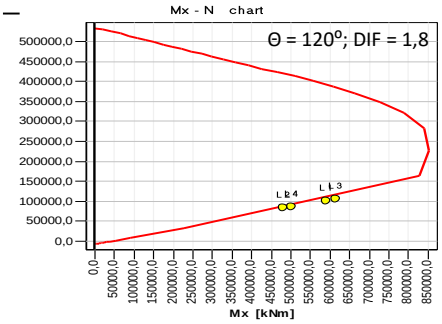

Figure 5.3: Effect vs strength - Grade C80/95

Section behavior in intermediate pre-failure shall provide advantage of stability during the dynamics to statics transition process.

Quasi-static structural answer:

The elapsed of dynamic response to impulsive force of implosion, forces mechanical properties to rearrange in the way to a quasi-static regime.

Local stress concentration once started at the sharp edges of implosion notch border favors the progression of concrete failure.

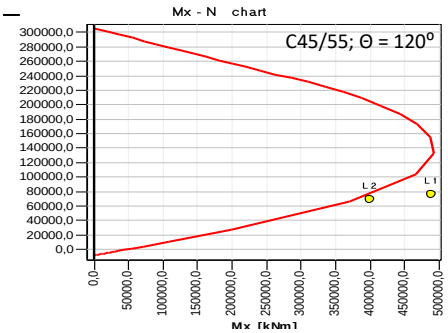

Figure 5.4: Effect vs strength - Grade C45/55

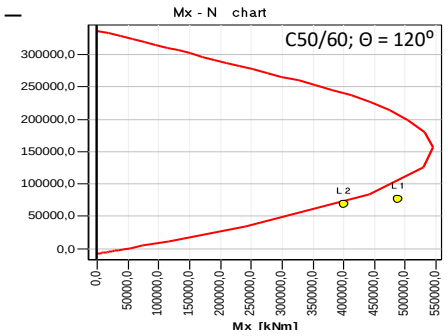

Figure 5.5: Effect vs strength - Grade C50/60

Note that in the case of pre-failure, progression to failure is non-reversible due to the increase of deformation up to material depletion which is facilitated by inertia forces emergence.

5.2 Equilibrium ultimate limit state

The comparison of inertia factors that activate the mechanism for the situation ante- vs post-implosion reflects the safety factor related to the overturning limit state.

$$FS = max\left(\frac{a_{II}}{a_I}\right) = 0.311 \rightarrow \frac{R_d}{E_d} < 1$$

The ratio satisfies to equilibrium ultimate limit state in terms of controlled demolition approach.

5.3 Finite-Element modelling

To determine stress and strain fields and predict structure damages after implosion, a model was built to run by SAP2000 v.23.2.0, based on the FEM (Finite Element Method). Accordingly, a reduced 30 m length of the stack (to limit the involved database), applied free-body resultant at top section center of gravity of top section and replication of geometric-mechanical properties.

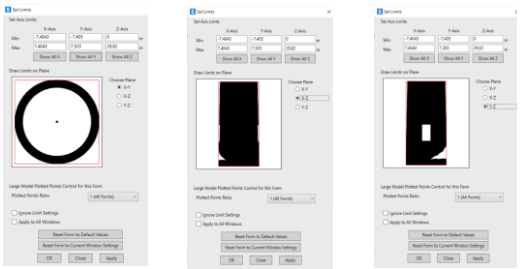

Figure 5.6: Model geometrical properties (SAP2000)

To understand the structural behavior compliant with different mechanical properties it is justified to include in analysis procedure two scenarios, respectively for minor and major characteristic concrete compressive strength.

Table 5.2: Post-implosion design scenarios

Concrete Grade	Gravity Load	Scenario
C45/55	1.1 F_{sy}	A
C50/60	0.9 F_{sy}	B

5.4 Compression stress fields

The analysis indicates the region with very high concentration of compression local stresses in the inner concave edge of the exposed surface of the stack, after implosion.

This stress intensity $\sigma_{33} = -91.6\ MPa$ implies failure. Scenario B is conditioning with the lower ratio $\frac{\sigma_{33,max}}{fck} \sim 1.8$ that seems first to be enough but shall be revised as the confinement state modifies concrete mechanical properties.

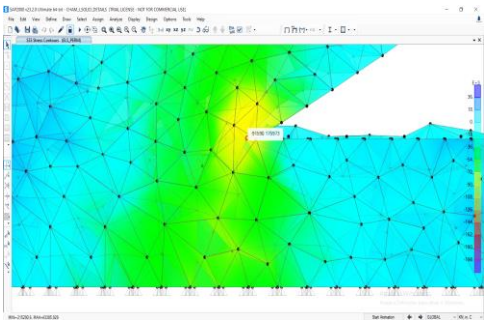

Figure 5.7: Compression stress concentration (SAP2000)

In-plane confinement stress $\sigma_{11} \neq \sigma_{22}$ therefore the minor value is used: $\sigma_{11} = -5.4\ MPa$.

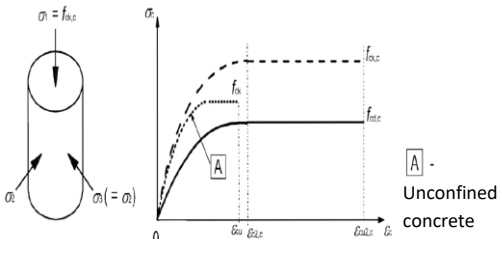

Figure 5.8: Stress-strain diagram for confined concrete [8]

This confinement stress effect, accordingly to the EC-2 approach, assigns to concrete Grade 50/60 a strength increment of about 40%.

$$f_{ck,c} = -70\ MPa\ ;\ (\sim 0.75 \cdot \sigma_{33})$$

5.5 Tensile stress fields

In Scenario B, the equivalent Von Mises tensile design stress is $\bar{\sigma}_{VM} = 21.6\ MPa$.

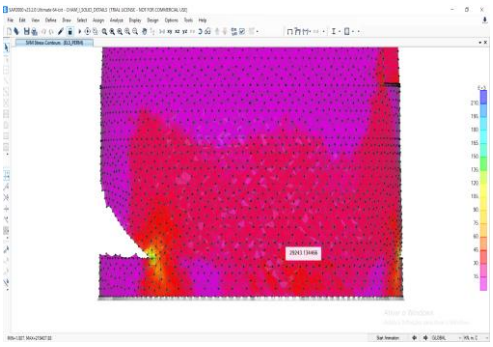

Figure 5.9: Equivalent Von Mises stress (SAP2000)

The strength of inner layer reinforcement in the residual cross-section vs the tensile effect:

$$\frac{R_d}{E_d} = \frac{1074\ kN/m}{11880\ kN/m} = 0.1$$

Hence, each steel bar acts as a structural fuse.

6 Final considerations

6.1 State-of-Art of main concepts

Concept C1:

This is a well-known practiced concept in the United States for controlled demolition of high-rise chimneys. It is supported by advanced non-linear analysis software tool based on the AEM (Applied Element Method).

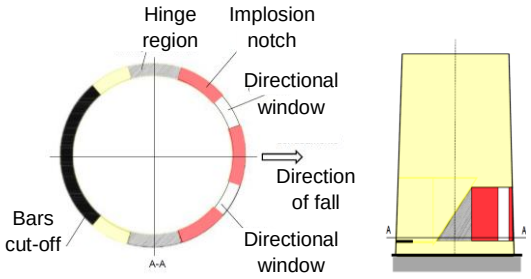

Figure 6.1: Modelling scheme of Concept C1 [7]

Concept C2:

This concept has been developed by structural engineers in China. Its main fundamentals differ from those of Concept C1 but key-parameters are common as the notch implosion geometrical arrangement assorted with directional windows.

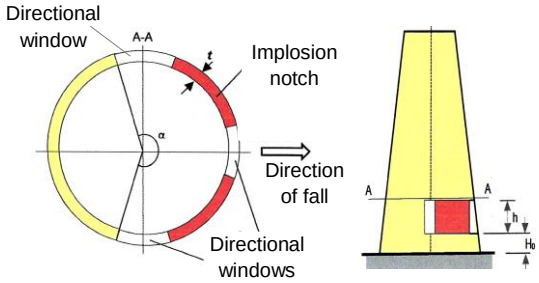

Figure 6.2: Modelling scheme of Concept C2 [18]

Concept C3:

This concept refers to the case analyzed in this dissertation. Pre-weakening work includes the two opposite windows and reinforcement cut-off of the outer layer in residual cross-section.

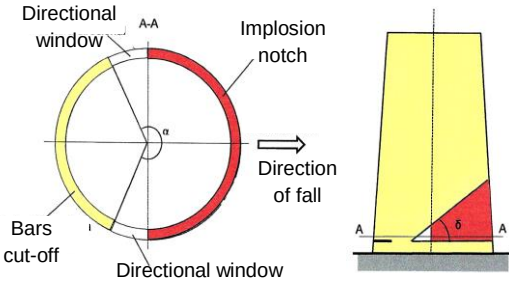

Figure 6.3: Modelling scheme of Concept C3 [15]

To outline, there is more than one concept to be used for controlled demolition of tall slender structures overturning. For this method, each different in-use technique is associated to the engineering concept that differs each case.

6.2 Additional considerations

Controlled demolition is the unique acceptable process to demolish tall slender structures. In large densified cities or infra-structure proximity, restriction on space around requires the use of the explosives technology to attend to minimum available close-off surface of debris deposition resultant from the impact of the structure to soil.

6.3 Future developments

In the future, controlled demolition engineering will be more and more solicited to give answers to the requisites of urban development, high-rise construction and reusing materials.

At the present time, technical and technological research in the domain of controlled demolition is without limits.

References

[1] Biggs, J. M. (1964). Introduction to structural dynamics. McGraw-Hill, New York.

[2] Chen D. et al (2014). A study on stress-strain testing of controlled blasting demolition of 210m chimney. 7th. Conference ICTA, Changsha.

[3] CEB - Comité Euro-International du Béton. Concrete structures under impact and impulsive loading. B.I. Nº 187 (1988), Dubrovnik.

[4] Chopra, A.K. (1995). Dynamics of structures, 4th ed. (2012). Prentice Hall Publishers, Boston.

[5] Clough, R. e Penzien, J. (1975). Dynamic of structures, 3rd ed. (2003). C&S Inc., Berkeley.

[6] Dyrbye, C. e Hansen, S. O. (1997). Wind loads on structures. J. Wiley & Sons, London.

[7] Elfouly, A. (2020). How the hinge method for controlled demolition works. Construction Pros LLC, NDA, Washington.

[8] Eurocode 1-6, EN 1991-1-6:2005. Actions on structures, Part 1-6. CEN, Brussels.

[9] Eurocode 2-1, EN 1992-1-1:2004. Design of concrete structures, Part 1-1. CEN, Brussels.

[10] Eurocode 8-6, EN 1998-6:2005. Design of structures for earthquake resistance: towers, masts and chimneys. CEN, Brussels.

[11] Eurocódigo 0, NP EN 1990:2009. Bases para o projecto de estruturas. IPQ (2009), Caparica.

[12] Eurocódigo 1-4, NP EN 1991-1-4:2010. Ações em estruturas, Parte 1-4. IPQ, Caparica.

[13] Li, S. et al. (2012). Failure law of supporting part of reinforced concrete chimney by blasting demolition. AMM, 170-173 (2012), 3250-3254, Trans Tech Publications, Bach.

[14] Niemann, H.-J.; Kasperski, M. (1999). Interference effects for a group of two reinforced concrete chimneys. JFS, 13 (1999), 987-997, Elsevier, Amsterdam.

[15] Rodrigues, R. V. et al. (2020). Demolição por derrubamento das chaminés da Central Termoelétrica de Setúbal. Congresso Nacional Reabilitar & Betão Estrutural, LNEC, Lisboa.

[16] Ruscheweyh, H. (1990). Practical experiences with wind-induced vibrations. JWEI, 33 (1990), 211-218, Aachen.

[17] Zdravkovich, M. M. (1988). Review of interference-induced oscillations in flow past two parallel circular cylinders in various arrangements. JWEIA, 28 (1988), 183-200, Amsterdam.

[18] Zhang, Z. (2016). Special blasting techniques. Rock fracture and blasting, theory and applications, ch. 25, 483-491, Elsevier, Amsterdam.

Web pages:

https://earth.google.com/web/@38.51003343,-8.84391923,23.23628236a.
Consulted in: 28.03.2021.

http://sig.mun-setubal.pt/websigsetubal/.
Consulted in: 13.04.2021.